ERDC/GSL TR-08-2

Geotechnical and Structures Laboratory

US Army Corps
of Engineers®
Engineer Research and
Development Center

Mechanical and Physical Properties of ASTM C33 Sand

Ernest S. Berney IV and Donald M. Smith

February 2008

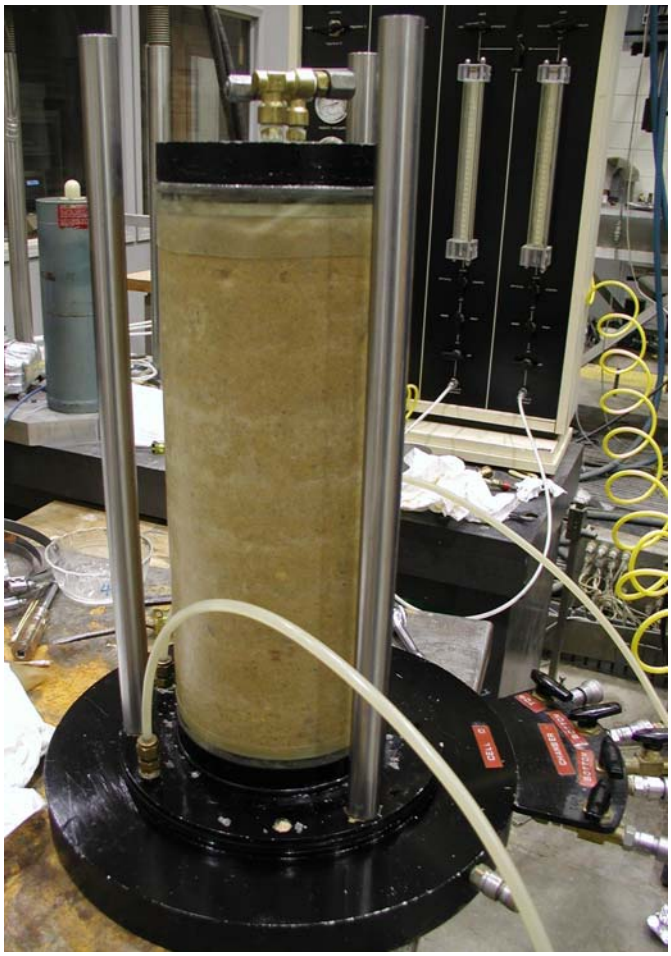

ERDC/GSL TR-08-2
February 2008

Mechanical and Physical Properties of ASTM C33 Sand

Ernest S. Berney IV and Donald M. Smith

Geotechnical and Structures Laboratory
U.S. Army Engineer Research and Development Center
3909 Halls Ferry Road
Vicksburg, MS 39180-6199

Final report

Prepared for Headquarters, U.S. Army Corps of Engineers
Washington, DC 20314-1000

Abstract: Determining the state of the ground is critical for Objective Force operations. Currently, no methods exist to remotely, and accurately, measure the near-surface soil properties (strength, density, compressibility, and texture) needed to define ground state. Analysis of low-velocity impact probe deceleration, obtained during penetration, is the most practical method to remotely determine ground state. Development of the physics describing the behavior of the impact requires in-depth knowledge of the physical properties of the relevant soil. This report provides an extensive suite of calibration and verification material properties for predicting the response of an ASTM C33 sand to low-velocity probe penetration. The experimental program determined the following physical properties for this sand: elastic behavior (shear and Young's moduli and Poisson's ratio), strength characteristics (friction angle, cohesion, compressibility, and triaxial strength), and construction parameters (maximum/minimum densities, optimum moisture content, and California bearing ratio).

Contents

Figures and Tables

Figures

Tables

Preface

The tests and results presented herein describe the results of the research effort entitled “Soil Properties from Low-Velocity Probe Penetration.” The objective of this research effort is to provide a physical model of low-velocity probe penetration to characterize soil by type, strength, maximum compaction, and initial density.

This work was conducted under the AT22 research program Advanced Penetrometer Technology at the U.S. Army Engineer Research and Development Center (ERDC). This project is part of a 3-year study that ended in 2007. This research program was sponsored by Headquarters, U.S. Army Corps of Engineers, Washington, DC.

This publication was prepared by personnel of the ERDC Geotechnical and Structures Laboratory (GSL), Vicksburg, MS. The findings presented are based upon laboratory experimentation conducted over a 6-month period in 2003. The principal investigator for this study was Dr. Ernest S. Berney IV, Airfields and Pavements Branch (APB), Engineering Systems and Materials Division (ESMD), GSL. Other ERDC personnel who assisted in the research include Dr. Jerome B. Johnson, Cold Regions Research and Engineering Laboratory; Drs. James D. Cargile and Donald M. Smith, GSL; and Charles Carter and Larry Dunbar, GSL.

Drs. Berney and Smith prepared this publication under the supervision of Don R. Alexander, Chief, APB; Dr. Larry N. Lynch, Chief, ESMD; Dr. William P. Grogan, Deputy Director, GSL; and Dr. David W. Pittman, Director, GSL.

COL Richard B. Jenkins was Commander and Executive Director of ERDC. Dr. James R. Houston was Director.

Recommended changes for improving this publication in content and/or format should be submitted on DA Form 2028 (Recommended Changes to Publications and Blank Forms) and forwarded to Headquarters, U.S. Army Corps of Engineers, ATTN: CECW-EWS, Kingman Building, Room 321, 7701 Telegraph Road, Alexandria, VA 22315.

Unit Conversion Factors

Multiply	By	To Obtain
cubic feet	0.02831685	cubic meters
cubic inches	1.6387064 E-05	cubic meters
degrees (angle)	0.01745329	radians
degrees Fahrenheit	(F-32)/1.8	degrees Celsius
feet	0.3048	meters
inches	0.0254	meters
inch-pounds (force)	0.1129848	newton meters
pounds (force)	4.448222	newtons
pounds (force) per square foot (psf)	47.88026	pascals
pounds (force) per square inch (psi)	6.894757	kilopascals
pounds (mass)	0.45359237	kilograms
pounds (mass) per cubic foot (pcf)	16.01846	kilograms per cubic meter
square inches	6.4516 E-04	square meters

1 Introduction

Background

Determining the state of the ground is critical for Objective Force operations. Currently, no methods exist to remotely, and accurately, measure the near-surface soil (NSS) properties (strength, density, compressibility, and texture) needed to define ground state. Analysis of low-velocity impact probe deceleration, obtained during penetration, is the most practical method to remotely determine ground state. However, the lack of physics-based interpretation theory (where each of the acting mechanisms is identified and determined separately) limits the accuracy of interpreting probe measurements.

Prediction of probe performance or inference of NSS properties from probe measurements is accomplished using numerical methods or a penetration theory. Penetration theories can be purely empirical, empirical with physical elements, or purely physical.

The most comprehensive method to analyze penetration problems is the numerical approach using finite-element, finite-difference, smoothed particle hydrodynamics, or other codes. Numerical methods solve the continuity, momentum, and energy balance equations of continuum mechanics in conjunction with an appropriate constitutive representation for the target materials of interest. These first-principle techniques can use a wide variety of initial and boundary conditions to simulate the penetration event. The constitutive material models that are used with the numerical methods must capture the appropriate responses of the target material. The material property data required for use in the numerical methods must be obtained from the appropriate independent laboratory tests on the target materials. The combined effects of soil strength, compaction, inertia, and probe design are not easily distinguishable except through computationally intensive, nonunique trial-and-error iterative methods, making it extremely difficult to determine soil properties from probe deceleration data.

Existing empirical models are based on experimental correlations of parameters such as penetration depth, crater volume, impact velocity or momentum, probe geometry, or other measurable quantities and generally

offer little insight to the physical processes that are occurring. These models can accurately predict penetration depth when information about the probe and the target material is within the range of experimental data used to develop the model (Backman and Goldsmith 1978, Young 1997). Empirical models are not suitable for inferring detailed material properties because the physical processes are hidden within the correlation "index" coefficients or simplified material descriptions.

Empirical models with physical elements are generally analytical models that provide correlations, such as those from empirical studies, but introduce relations between parameters of the system on the basis of physical requirements. The best known such relation is a resistive force that is a function of the projectile velocity where the coefficients are associated with frictional and added mass effects (Backman and Goldsmith 1978). While better than empirical models, these models are also not well suited for inferring NSS properties from penetration measurements because their coefficients are essentially free parameters set through correlation with experiments.

A purely physical approach uses experimental observations to guide the formulation of an ideal model of the processes that produce resistance forces on a probe. Existing physical models generally oversimplify the deformation geometry and do not include all relevant physics.

While the number of penetration experiments that have been conducted is large, the number of direct observations of the controlling physical processes is limited. Available data indicate that, at ordnance velocities, penetration resistance forces can arise from the failure and compaction of the initially undeformed soil, added mass effects, soil particle comminution, friction between the probe and soil, and failure within the compacted soil region (Allen et al. 1957, Anderson et al. 1996, Backman and Goldsmith 1978, Johnson 2001). Furthermore, the shape of the probe tip determines the partition of importance of probe-soil friction, soil strength, and the geometry of the zone of compacted soil around a probe. NSS deformation is primarily normal to the probe surface (Gill 1968) but can be moderated by friction between the soil and probe surface.[1]

[1] Johnson, J. B., J. D. Cargile, and D. M. Smith. 2004. Soil properties from a low-velocity probe. Presentation of progress, ERDC Program Review. Vicksburg, MS: U.S. Army Engineer Research and Development Center.

Objective

The objective of this research was to provide calibration and verification material properties for predicting the response of unbound granular materials to low-velocity probe penetration.

Scope of work

This research addresses the laboratory tests and results for an ASTM C33 concrete sand used in the initial trial tests of the low-velocity probe penetrator. This sand was the unbound granular material chosen for study because of its ease of availability. Historical test data on its material properties were supplemented with additional laboratory testing to provide essential features of soil response required for numerical modeling. These essential features include state, modulus, yield strength, nonlinear elastic response, permanent or plastic deformations after yield, cyclic loading, strain softening/hardening, and shear dilatancy.

2 Problem Statement

The success of the Future Force will depend largely on the ability to remotely depict the battlefield environment prior to initiating military operations. Future Force requirements to deploy a Stryker Brigade Combat Team within 96 hr and/or one Division within 120 hr in temperate and cold regions make it imperative that a system be available to remotely assess the material properties of soils and pavement structures in the region of operations. Accurate site-specific information about the state of the ground (strength, compaction, initial density, elastic modulus) can best be obtained by directly probing the ground using an instrumented ballistic penetrator. Determining the load-carrying capacity of a natural (unprepared) landing site is an extremely complex issue requiring an accurate, rapid assessment of the soil strength profile (at the surface and with depth). Military personnel can be used to obtain this information but at a substantial risk of casualty or capture, or inability to obtain sufficient information.

The limits of using a low-velocity probe to determine soil properties depend directly on the accuracy of the physical penetration model, deceleration measurement resolution, and the understanding of the relationship between soil properties and probe deceleration. It is not possible to accurately characterize soil properties without a physical model because of the combination of effects from the probe (geometry, cone half-angle, mass, impact velocity) and soil (initial density, strength, compaction, probe/soil friction, particle size) that affect probe deceleration. To extract soil properties information from the probe deceleration record requires that the effects of the probe and soil must be distinguishable from each other. The physical model can separately account for the probe effects (which are uniquely known) and inertia, allowing interpretation efforts to focus on the soil. However, even with an accurate physical model, it is not possible to uniquely characterize soil properties, without further reducing the number of unknown variables by bringing additional information into the interpretation process. This information includes using the knowledge that (1) different soil types yield distinct deceleration histories related to strength and grain size, (2) particle packing experiments and theory place an upper bound on maximum compaction fractional density, and

(3) California bearing ratio (CBR) test and resilient modulus for soils can be related to soil strength.

Resilient modulus of subgrade soils is an important factor in pavement design/evaluation and mobility analysis and is typically evaluated using simple empirical relationships with CBR values. Studies have indicated that both the resilient modulus and CBR are related to the undrained soil shear strength, and hence to each other (Black 1961, Duncan and Buchignani 1976, Thompson and Robnett 1979). This implies that a relationship between probe-derived soil strength and the resilient modulus and CBR should exist, providing a pathway from soil properties derived from low-velocity probe measurements to the resilient modulus and CBR.

A physically based model of low-velocity probe penetration into soil has been developed using the essential factors that control probe deceleration through transference of probe momentum to the soil. Probe momentum is lost due to soil failure processes at the outer edge of the zone of compacted soil around the probe (soil strength), compaction and acceleration of the soil particles after failure (soil inertia), and sliding between the probe and surrounding soil (friction).

Improvements to the model will require experiments to improve our understanding of near-surface soil failure processes that produce cratering, as well as the effects of soil type and texture on the magnitude and overall deceleration history of a probe. High-quality laboratory test data are needed to enable these refinements to be made.

3 Laboratory Tests and Results

Overview

In order to apply a numerical model for prediction of material response under load, the model must be calibrated from laboratory data. The parameters for material strength, failure, and deformation that define model properties must be determined. This chapter provides detailed laboratory tests and analyses that can be used to achieve proper calibration for an ASTM C33 concrete sand.

The material

A poorly graded concrete sand (SP) meeting ASTM C33 requirements was selected as the test material. This material is available in large quantities from a local aggregate supplier, which makes it ideal for construction of large test beds. The soil has uniform consistency from the supplier, ensuring a steady supply of material and the ability to construct repeatable specimens. The concrete sand is a nonplastic soil with a minimum of fines (2.5% finer than the No. 200 sieve) and a minimum of gravel (6.3% greater than the No. 4 sieve). These characteristics make the soil a good choice for this study because its mechanical response is solely dependent on the frictional behavior of the soil (reducing the number of variables to analyze), and the lack of large coarse aggregate will enable optimum penetration of the probe.

The test program

An outline of the laboratory work conducted as part of this study follows. The laboratory program was begun in January 2003 and completed in May 2003.

Tests conducted

Specific Gravity (1) (ASTM D 854)

1 test run on total sand sample

Grain-size Distribution (1) (ASTM D 422)

1 test run on total sand sample

Proctor Density Curves (2) (ASTM D 698 and D 1557)

Set of 6 points using modified energy – 56 blows, 5 layers, 10-lb hammer
Set of 6 points using standard energy – 25 blows, 3 layers, 5.5-lb hammer

California Bearing Ratio (17) (ASTM D1883)

Set of 6 points using modified energy
Set of 6 points using standard energy
Set of 5 points at the maximum relative density

Relative Density (5) (ASTM D 4253 and D 4254)

5 sets of maximum and minimum density tests performed at water contents of 0%, 2%, 4%, 6%, and 8%

Direct Shear Test (12) (ASTM D 3080)

4 tests run (3 at maximum and 1 at minimum density) at 50 psi normal stress
4 tests run (3 at maximum and 1 at minimum density) at 100 psi normal stress
4 tests run (3 at maximum and 1 at minimum density) at 200 psi normal stress

Isotropic Consolidation Test (4) (ASTM D 2435)

Conducted as part of each consolidated undrained (CU) test

Consolidated Undrained (CU) Triaxial Saturated Test with Pore-pressure measurements (4) (ASTM D 4767)

1 test run on modified energy Proctor sample at 15 psi effective confinement

1 test run on modified energy Proctor sample at 50 psi effective confinement
1 test run on modified energy Proctor sample at 100 psi effective confinement
1 test run on modified energy Proctor sample at 150 psi effective confinement

Consolidated Drained (CD) Triaxial Saturated Test (no volume change measurements) (4) (ASTM D 4767)

1 test run on modified energy Proctor sample at 15 psi effective confinement
1 test run on modified energy Proctor sample at 50 psi effective confinement
1 test run on modified energy Proctor sample at 100 psi effective confinement
1 test run on modified energy Proctor sample at 150 psi effective confinement

Modified Consolidated Undrained (CU-Q) Triaxial Test (4)

All tests conducted at 10 psi confining pressure

1 test run on modified energy Proctor sample at 2% water content
1 test run on modified energy Proctor sample at 3% water content
1 test run on modified energy Proctor sample at 4% water content
1 test run on modified energy Proctor sample at 5% water content

Index properties and grain size distribution

Tests of specific gravity and grain size distribution, including a hydrometer analysis, were conducted to allow Unified Soil Classification System (USCS) classification of the soil and to establish its gradation relative to the fine aggregate limits for concrete defined in ASTM C33. The grain size distribution for the tested concrete sand is shown in Figure 1, and its relative location with respect to the ASTM C33 bounds is shown. The specific gravity of the sand was determined to be 2.66, which is reasonable given the material is a silica-based sand. A summary of the index properties is shown as Table 1.

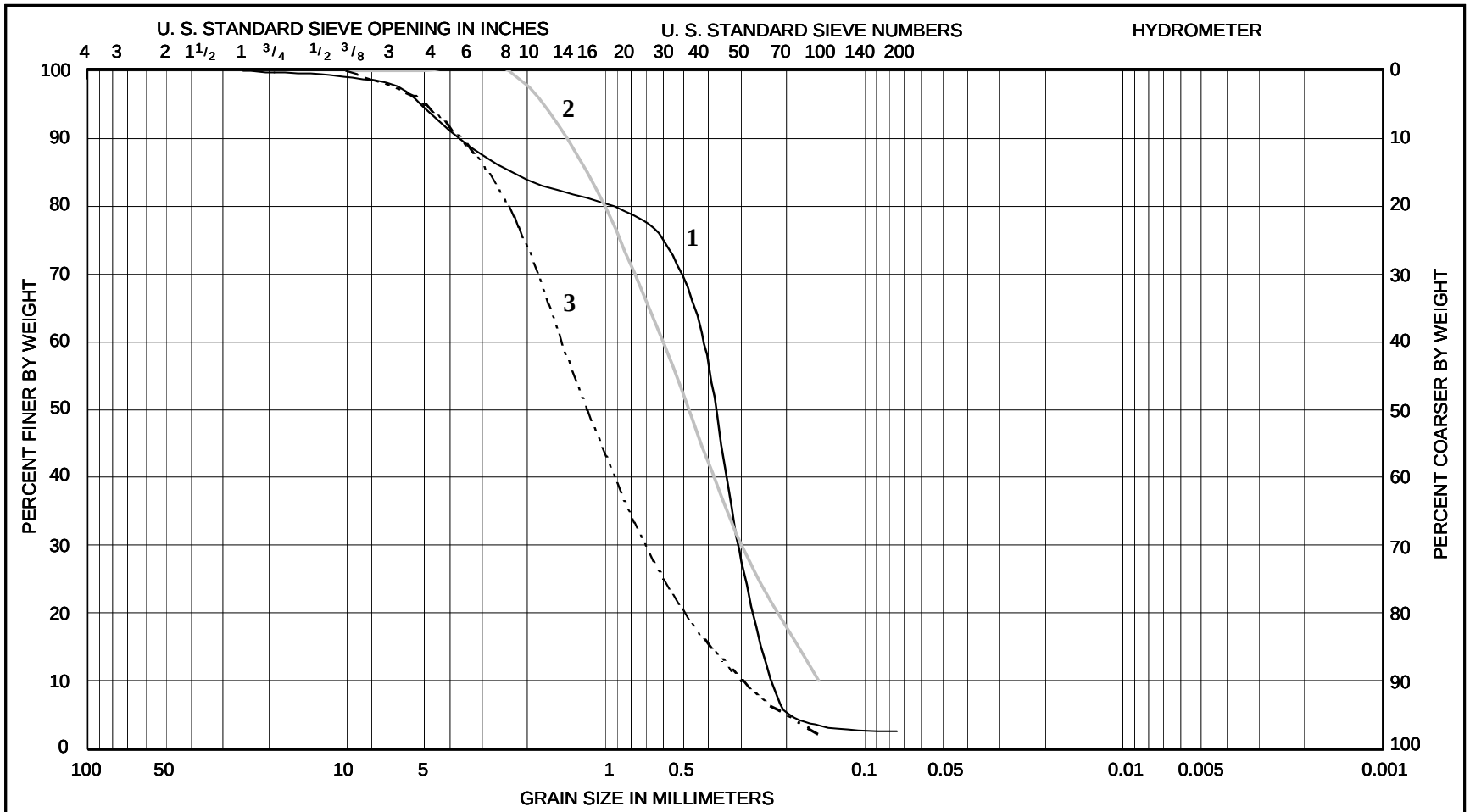

SAMPLE NO.	MATERIAL	CLASSIFICATION	NAT W%	LL	PL	PI
1	Concrete Sand	Sand with Gravel (SP)		NP	NP	NP
2	ASTM C33 Fine Aggregate Maximum					
3	ASTM C33 Fine Aggregate Minimum					

GRADATION CURVES

PROJECT	**Low Velocity Penetration Study**
SOURCE	**Local Vicksburg, MS**
DATE	**7 January 2003**

Figure 1. Grain size distribution for concrete sand.

Table 1. Summary of index properties for concrete sand.

Brown Sand with Gravel (SP) – Non Plastic	
Specific Gravity	2.66
Percent Gravel	6.3
Percent Sand	91.3
Percent Fines	2.4
Percent Silt	>80
Percent Clay	<20

This particular sample of concrete sand falls slightly out of the prescribed ASTM bounds in the coarse sand range (sieve Nos. 20 through 40) but is still considered a representative sample for a large batch of fine aggregate. The breakdown of the soil fractions by weight is 6.3% gravel, 91.3% sand, and 2.4% silty fines. (Less than 0.3% is of a clay-size fraction.)

Compaction and relative density

A series of compaction tests was conducted covering a range of moisture contents from 0% to 8%. Two levels of impact compaction energy were applied: standard and modified, according to ASTM test methods D 698, Method A, and D 1557, Method A (Figure 2 and Figure 3). A third level of energy was applied resulting from the vibratory compaction afforded by the relative density test that provided a soil matrix denser than modified Proctor (Figure 4). Because of the noncohesive nature of the SP material, a series of relative density tests measuring both minimum and maximum density were conducted at varying moisture contents. ASTM standards require that the sand be oven dried prior to testing, and this was carried out for the 0% water content case. However, to observe the influence of moisture directly on vibratory compaction and CBR strength, additional relative density tests were conducted with moisture added to the sand. A summary of the minimum and maximum densities is given in Table 2.

During Proctor compaction, both energy levels exhibited similar maximum densities, ranging between 110 and 112.5 pcf over the moisture range of interest. Compaction through the vibratory method yielded slightly larger densities, ranging between 110 and 114 pcf. This indicates that the compaction density of SP sand is insensitive to impact energy level and improved only slightly with vibration.

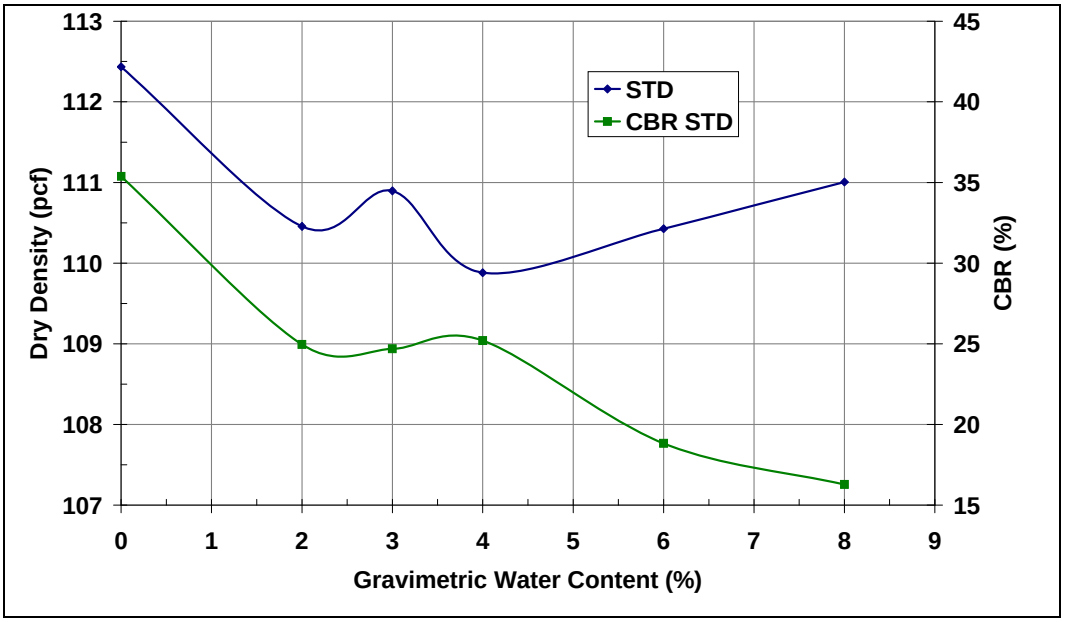

Figure 2. Standard Proctor laboratory compaction and CBR curve for SP.

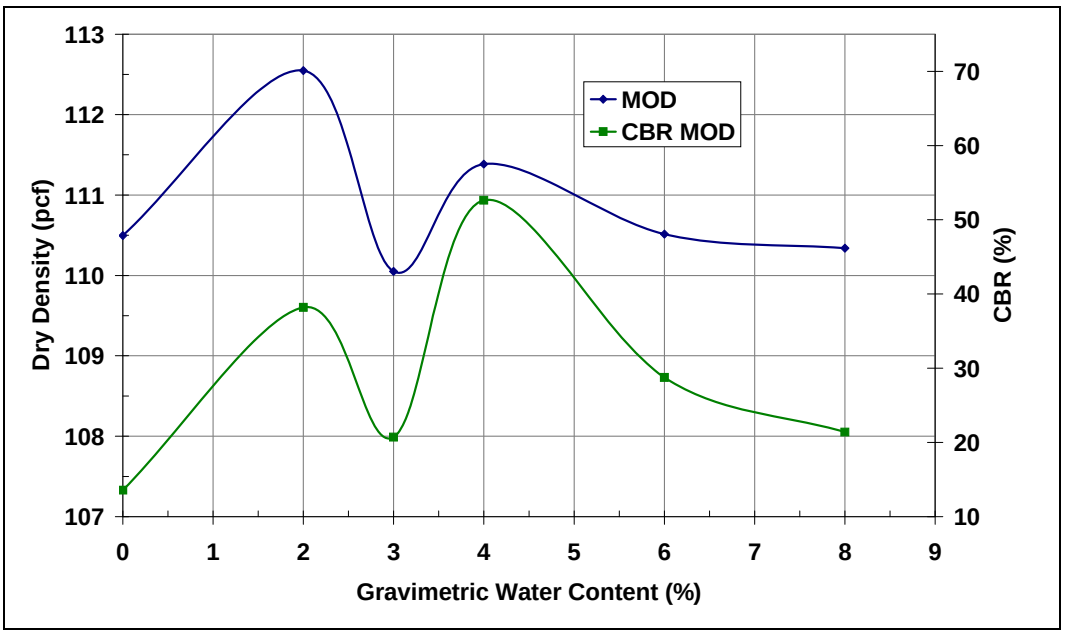

Figure 3. Modified Proctor laboratory compaction and CBR curve for SP.

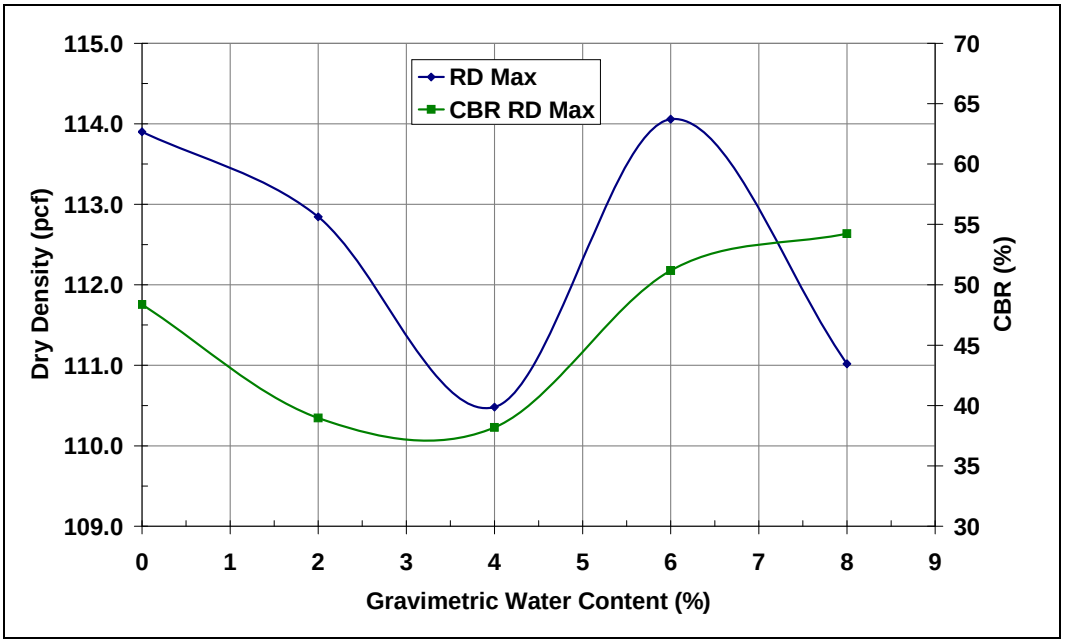

Figure 4. Maximum relative density laboratory compaction and CBR curve for SP.

Table 2. Relative density ranges for SP sand.

Water Content (%)	Maximum Density		Minimum Density	
	Dry Density (pcf)	Minimum Void Ratio	Dry Density (pcf)	Maximum Void Ratio
0	113.9	0.4573	96.9	0.7129
2	112.8	0.4709	70.4	1.3580
4	110.5	0.5024	65.3	1.5423
6	114.1	0.4553	67.5	1.4607
8	111.0	0.4951	63.9	1.5980

The CBR strength of the compacted sand had considerable variability during the Proctor compacted samples. Both Proctor samples yielded low-end CBR values near 15, although this occurred at both the driest and wettest condition for the modified energy level versus only at the wettest condition for the standard energy level. Peak CBR values were greater for modified than standard, being 50 and 25, respectively. Vibratory compacted specimens exhibited a narrower range of CBR values at an elevated level than those of the impact compacted specimens, ranging between 37 and 55. This suggests that the improved particle arrangement from vibratory compaction provides an improved frictional resistance to loading that is not captured at similar densities using an impact compaction method.

Direct shear

To evaluate the frictional response of the SP concrete sand, direct shear tests were performed at both the maximum and minimum relative densities to obtain a maximum and minimum friction angle for the sand. *These values can later be refined based upon the triaxial tests described later in this report.* Three replicates of the direct shear test were performed on the dense specimens along with one series at a loose density. Each specimen cell was a 3-in. × 3-in. square in area by 1 in. deep (Figure 5). To obtain a uniform sample height for loose and dense sand specimens, a cardboard grooving tool was constructed (Figure 5). This tool allowed the investigators to level the loosely placed sand and to smooth the rough surfaces of the densely compacted sand specimens. The results of these tests are shown in Figure 6 along with their corresponding friction angle. In summary, the frictional response of the SP sand varies between a maximum of approximately 40 deg and a minimum of 33 deg. This falls within the typical range of frictional response for rounded sandy soils with a maximum between 37 and 40 deg and a minimum between 30 and 34 deg with the higher values being present in well-graded sands (Lambe and Whitman 1969).

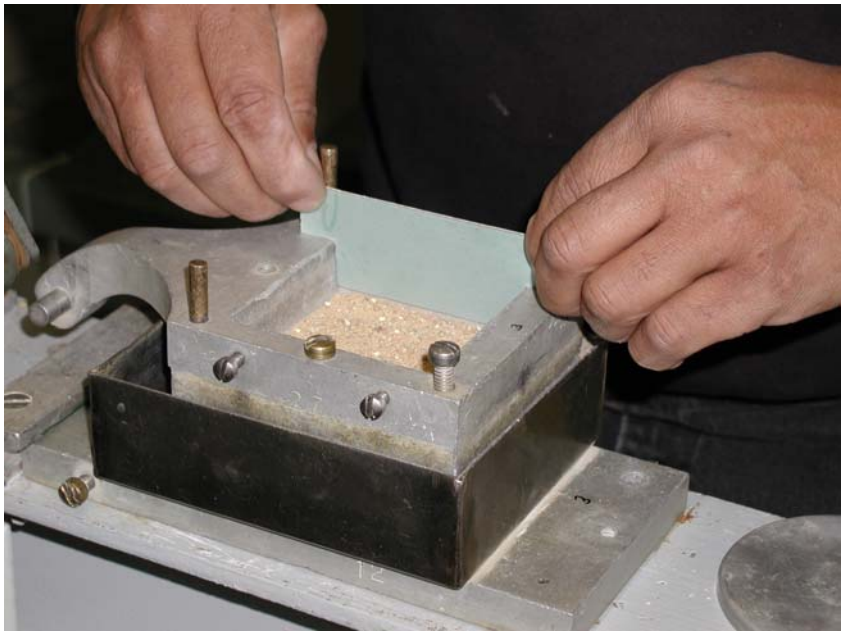

Figure 5. Grooving tool to smooth surface of sand layer in direct shear box.

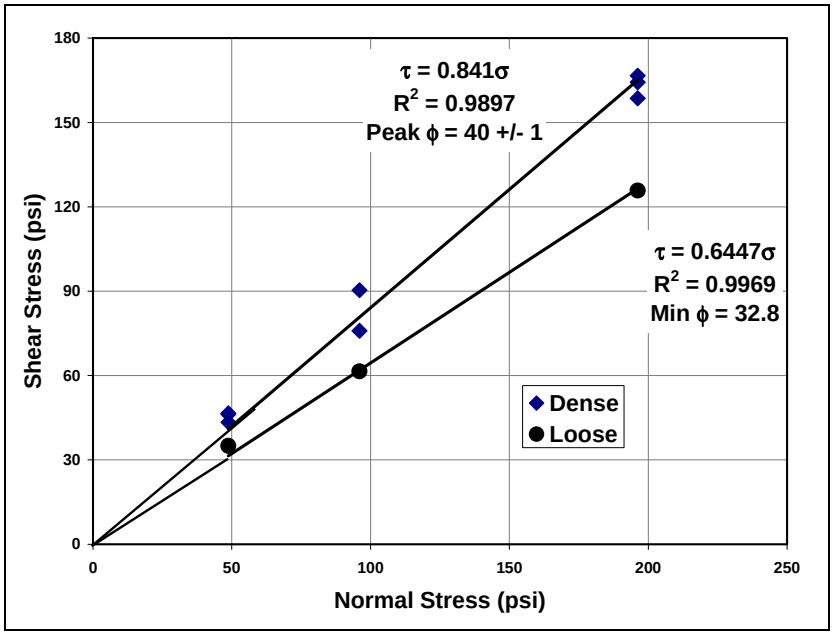

Figure 6. Direct shear analysis for SP sand.

Triaxial test

A cylindrical triaxial test was selected in which a test specimen is subjected simultaneously to axial stress and a radial stress (Figure 7). The radial pressure is generated by placing the specimen in a pressurized water bath enclosed in a steel-walled chamber (Figure 8). Axial load is generated by a hydraulic ram incorporated into the vessel. In general, three types of load paths can be obtained from such a device. These can be described in terms of principal stresses σ_1, σ_2, and σ_3 where ($\sigma_1 \geq \sigma_2 \geq \sigma_3$ with compression being a positive value of stress) it follows:

1. Hydrostatic (isotropic) compression – the axial stress is equal to the radial stress ($\sigma_1 = \sigma_2 = \sigma_3$).
2. Triaxial compression – the axial stress is greater than the radial stress ($\sigma_1 > \sigma_2 = \sigma_3$).
3. Triaxial extension – the axial stress is less than the radial stress ($\sigma_1 = \sigma_2 > \sigma_3$).

For the cylindrical triaxial test, two of the three principal stresses are equal at all times. For the research conducted in this study, load paths (1) and (2) are considered. The combination of these two tests is used to determine the strength and deformation properties in both hydrostatic and shear conditions, allowing a description of the material response during loading suitable for calibrating a variety of numerical models.

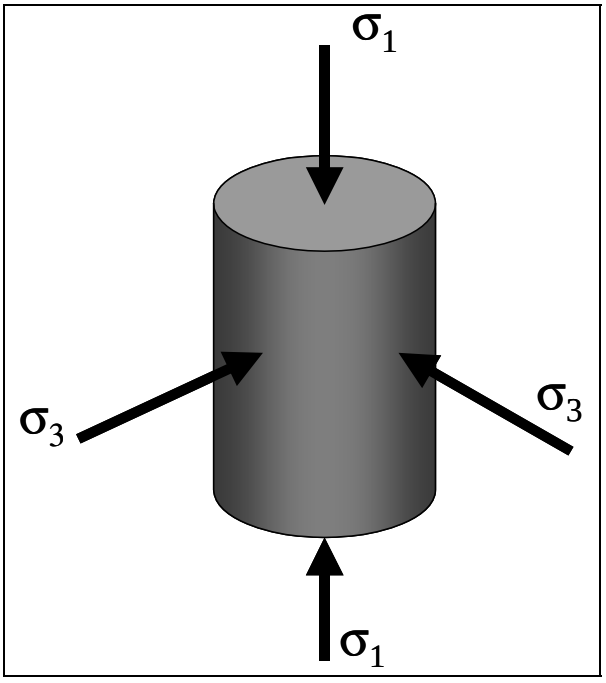

Figure 7. Principal stresses acting on cylindrical soil specimen during triaxial shear test.

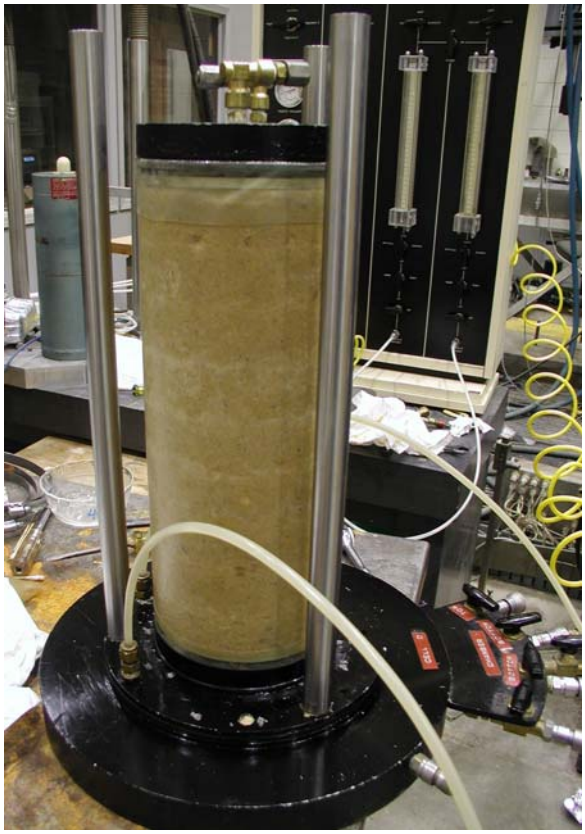

Figure 8. Triaxial specimen of SP sand after compaction.

Specimen preparation

Each triaxial specimen tested in this study was cylindrical in shape with an approximately 6.0-in. diameter by 13.5-in. height. To prepare the specimens, an appropriate mass of water was mixed by hand into an air-dried sample of SP sand. This mixture was then sealed in a plastic tub to allow the moisture to come to equilibrium within the mass of soil. An appropriate amount of moist soil was then weighed out and compacted using a Proctor hammer and rod to a height of 1.5 in. for each of nine lifts in a 6-in.-diam triaxial mold containing a thin latex membrane (Figure 8). Each specimen had its diameter determined as an average of six readings found from three positions along its height and at a rotation of 90 deg. The average overall height of each specimen was 13.4 in. ± 0.058 in. with a diameter of 6.026 in. ± 0.02 in. Specimens were weighed on a digital electronic scale with an accuracy of ±1 g. Initial water contents of each specimen were determined from trimmings collected after each specimen was prepared. Specific gravity, height, diameter, and the gravimetric water content were all used to calculate the initial void ratio of each specimen prior to any further testing.

Each specimen was fitted with a top and bottom filter paper and porous stone. The compaction process tended to cause small punctures in the latex membrane placed around the sample inside the triaxial mold. Therefore, a second thin latex membrane was placed around the extruded triaxial sample to minimize water permeating in or out of the specimen from the chamber fluid. Final preparation of the test specimen required covering the surface of the outer membrane with a layer of aluminum foil to minimize air diffusion during backpressure saturation and then a third thicker latex membrane placed over the top of the aluminum foil. To minimize the structural influence of the aluminum foil on the modulus of the soil sample, the foil was cut into 2-in.-wide by 13.5-in.-tall strips and placed vertically along the perimeter of the soil sample (Figure 9 and Figure 10). High confining pressures help to seal the aluminum foil strips around the sample.

End platens were placed on the top and bottom of specimens as they were mounted in the chamber. Prior to final chamber assembly, pore pressure and fluid volumes were monitored carefully to detect the possibility of leakage through the outer membrane. If any leaks were found, the specimens were removed and the damaged membrane(s) replaced. Final sealing of the specimen is shown in Figure 11.

Figure 9. Application of thicker outer latex membrane and aluminum foil strips to specimen to reduce air diffusion.

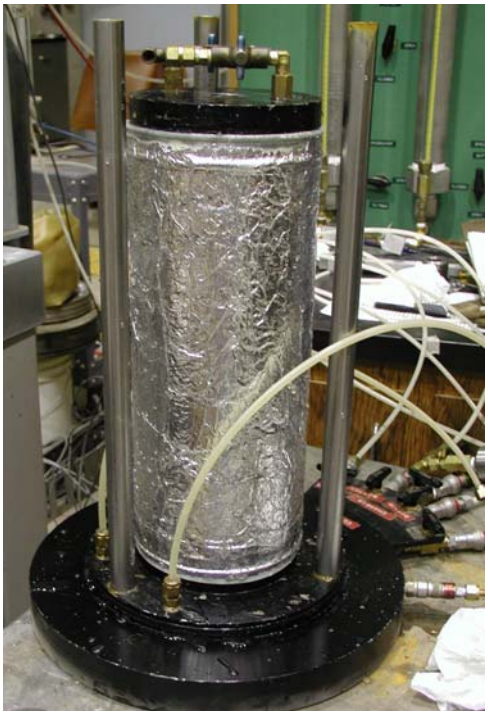

Figure 10. Completed SP triaxial specimen set-up with outer aluminum foil layer.

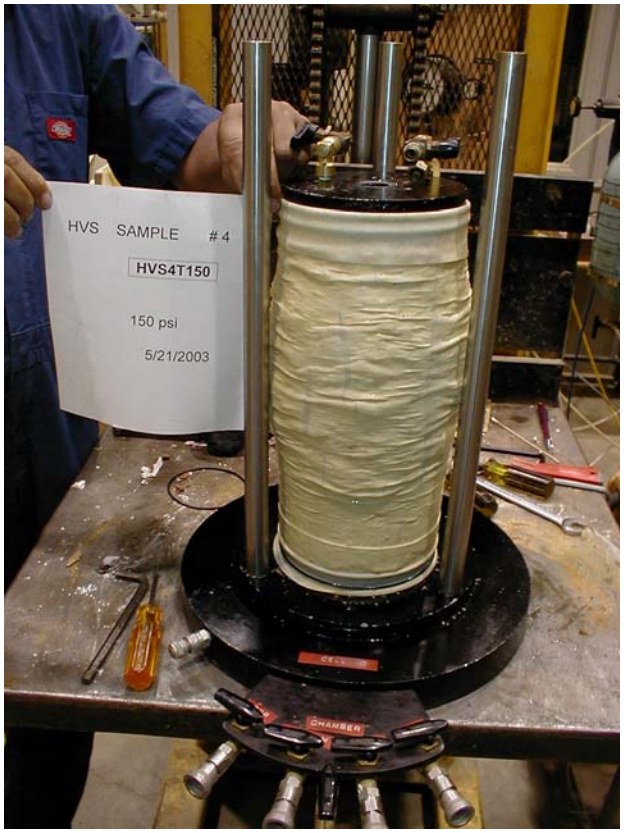

Figure 11. View of final membrane around specimen seen after failure.

Specimens were then de-aired by leaving chamber pressure at atmospheric and applying a vacuum at the top of the specimen no greater than –14 psi to ensure that the isotropic effective stress of the sample did not exceed 15 psi. This vacuum restriction ensured that all specimens to be tested at 15 psi effective confining pressure would not be overconsolidated. Specimens were saturated by drawing water through the soil using the applied vacuum. Water was drawn through the specimen until at least two full burettes (45 cc) of water had been passed through the specimen, at which point it was considered saturated. Axial deformation of the specimens due to swelling or collapse from de-airing/saturation was determined from a linear variable differential transformer (LVDT) placed along the loading piston, which had a rigid connection with the top platen in contact with the top of each specimen. The LVDT recorded the differential movement of the top of the specimen from an initial gauge reading with an accuracy of 0.001 in. (0.025 mm).

The chamber fluid was added to the triaxial chamber until filled, at which point a slight chamber pressure of 5 psi was applied while setting the

specimen's internal pressure to 2 psi, creating a nominal 3 psi effective mean confining stress. This slight confining pressure prevented damage to the membranes until the specimen was prepared for its target confining pressure. Any entrained air released into the sample during this reduction in effective confining pressure was removed by again flushing water through each specimen using a slight vacuum.

Once flushing was completed, each sample was backpressure saturated. The vacuum was reduced as the internal water pressure was increased, and the chamber pressure was increased such that the difference between the two pressures remained about 10 psi effective confinement. Back-pressure was increased until no additional water flowed into the system, at which point the stiffness of the fluid system was checked by measuring Skempton's B value (a ratio of pore pressure change to effective confining stress change) to determine whether a value of 0.95 had been achieved. If a value of 0.95 was not achieved, the backpressure was increased and the process was repeated. Measurements of axial deflection were taken before and after completion of the backsaturation stage to record changes in sample volume.

For purposes of developing the critical state strength envelope, it was preferable to have specimens at a variety of confining pressures. Once backpressure saturation was completed, the chamber pressure was then increased to one of four effective confining pressures (15, 50, 100, and 150 psi) for both drained and undrained triaxial specimens. These four pressures cover the expected range of tire pressures occurring on light infantry vehicles to heavily loaded military transport aircraft.

Isotropic (hydrostatic) consolidation test

A poorly graded sand exhibits little consolidation and elastic rebound when loaded isotropically. Therefore, the isotropic consolidation phase of loading was performed in a single loading step. The entire confining pressure was steadily increased to the prescribed value in a relatively short period of time with the assumption that consolidation occurs rapidly in the sand. Changes in sample height and volume were recorded at the end of applying this single loading step. A summary of the void ratios at initial compaction, after backpressure saturation, at the end of consolidation, and after drained shearing is provided as Table 3. Figure 12 shows the isotropic response in a void ratio-mean stress space.

Table 3. Summary of isotropic consolidation data.

	Void Ratio			
Specimen	After Compaction	After Backsaturation	After Consolidation	After Shear
Undrained				
15	0.547	0.539	0.538	0.538
50	0.537	0.527	0.528	0.528
100	0.532	0.533	0.523	0.523
150	0.539	0.536	0.525	0.525
Average	0.539	0.534	0.529	0.529
Std. Dev.	0.006	0.005	0.007	0.007
Drained				
15	0.535	0.532	0.531	0.582
50	0.553	0.547	0.541	0.554
100	0.540	0.537	0.528	0.557
150	0.545	0.543	0.529	0.537
Average	0.543	0.540	0.532	0.557
Std. Dev.	0.008	0.007	0.006	0.019

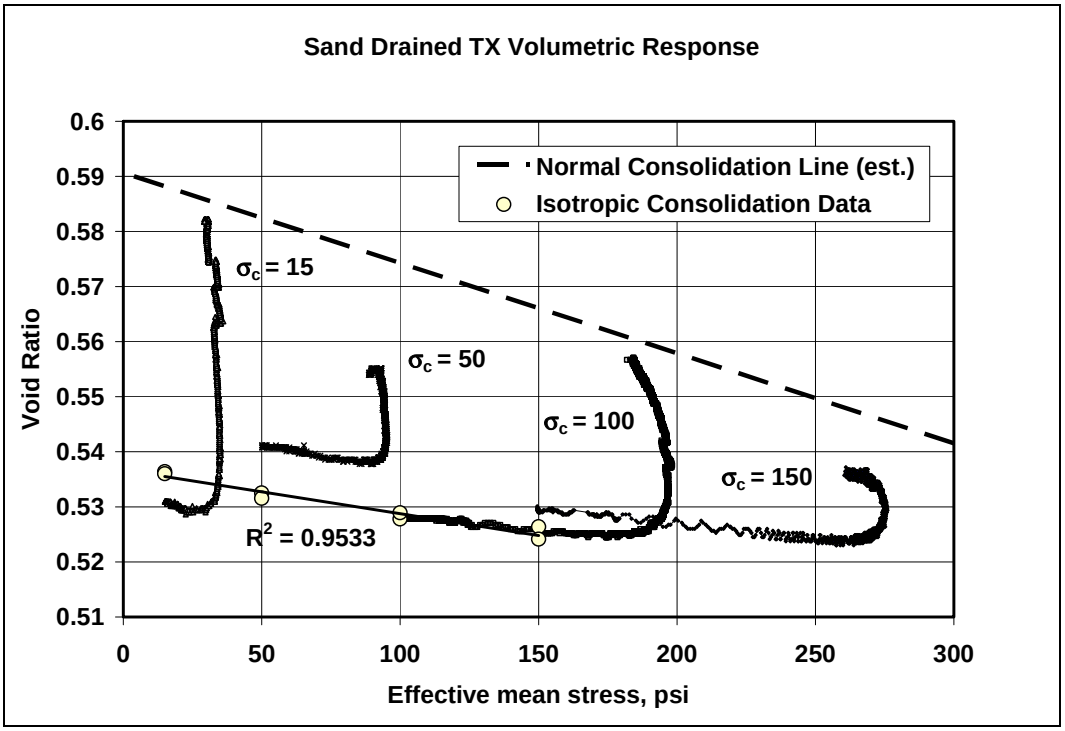

Figure 12. Drained and undrained isotropic and drained hydrostatic response for SP sand.

Triaxial shear

Once the final effective chamber pressure was reached and consolidation was completed, the axial load was increased until failure of the specimen in triaxial compression. For the undrained triaxial specimens, an electronic pore pressure transducer with a range of 200 psi and an accuracy of ±0.1 psi was saturated and then attached to the exit tubing of each specimen to monitor changes in pore pressure during the constant volume shearing. The load cell data, axial deflection, and pore pressure readings were electronically recorded.

Triaxial shearing of each specimen was conducted as per ASTM D 4767 at a rate of 0.01 mm/min for a time period of approximately 22 hr, at which time an axial strain of 20% was achieved and the samples had either failed or reached a critical state response. The specimens were then unloaded and the chambers removed from the mounting apparatus (Figure 11). In this process, the chamber pressure and backpressure were removed such that the backpressure never exceeded the chamber pressure. Each chamber was then drained of fluid, and the specimen was removed. An average post-test moisture content of the saturated soil was taken by drying the entire specimen. Figures 13-16 show the resulting shear strain-shear stress-volumetric strain behavior of specimens during the triaxial test where shear stress $q = \sigma_1 - \sigma_3$. Figure 17 shows the resulting effective stress path plot for all drained and undrained triaxial specimens.

Of interest during testing was that the 150 psi undrained test specimen experienced a sudden loss of axial loading early in the shearing phase of the test and therefore experienced a hysteretic loop in its response, as shown in Figure 18. This cyclic load proved valuable for analysis as it provides a measure of the effective stress elastic shear modulus, G, at small strain levels. The hysteretic response of the 150 psi undrained sample occurred at a shear strain magnitude (1.5%) much less than at failure. Therefore, the elastic response of the material is well represented at this strain level. A line drawn as shown in Figure 18 represents twice the shear modulus, $2G$. Taking two points lying along the line, each with coordinates (shear strain, shear stress) of (1.2327%, 6.5 psi) and (1.8492%, 193.1 psi), one obtains an effective stress elastic G = 15,215 psi. This compares best to a G obtained at a shear strain of 0.3% (G = 15,488 psi) (Figure 19).

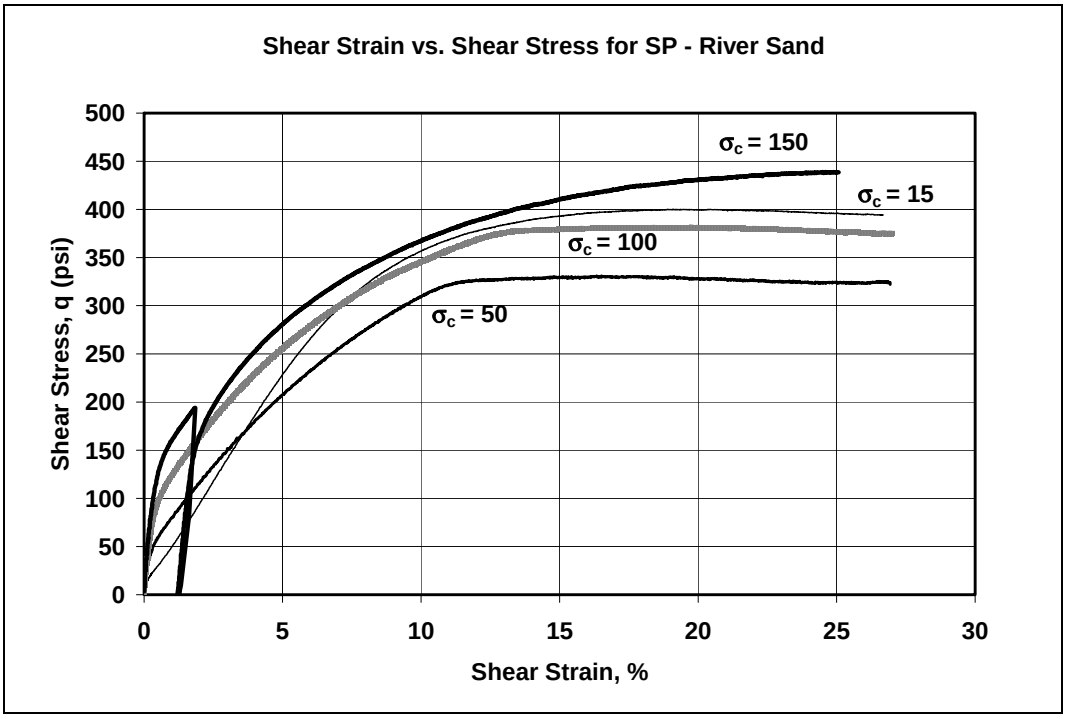

Figure 13. Undrained shear stress-shear strain response for SP sand.

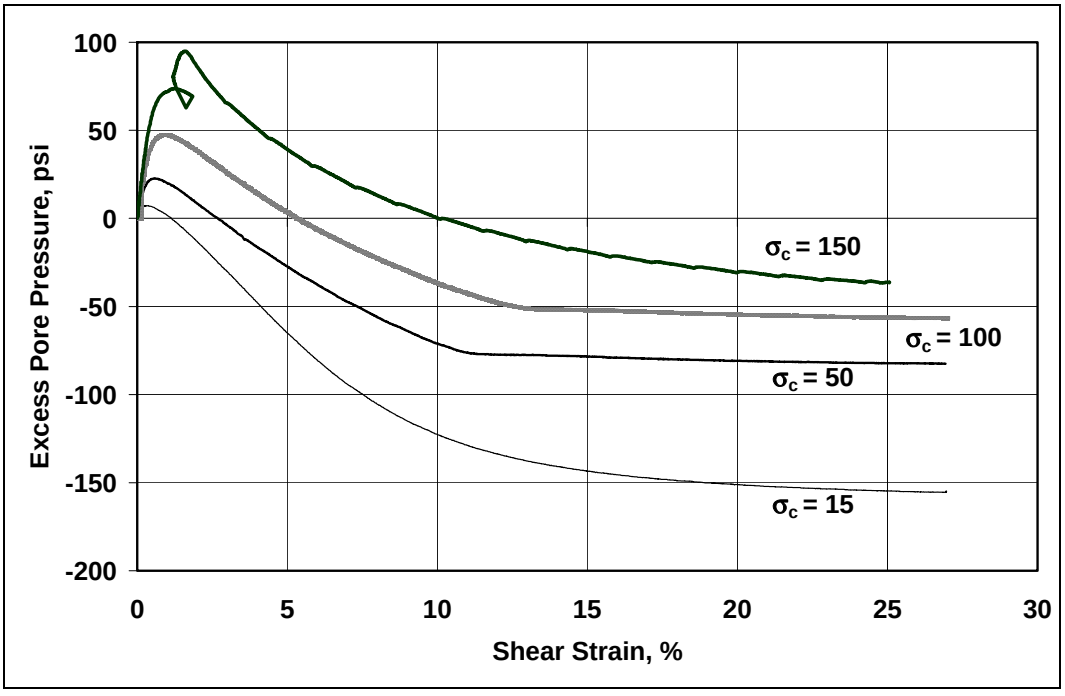

Figure 14. Undrained pore pressure-shear strain response for SP sand.

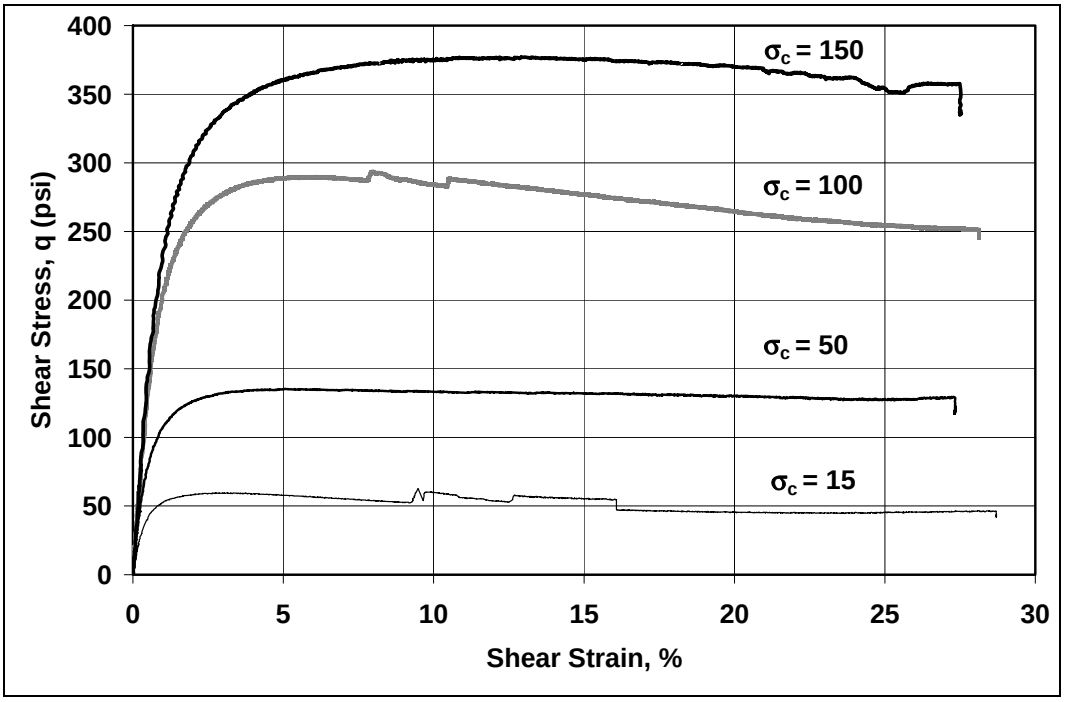

Figure 15. Drained shear stress-shear strain response for SP sand.

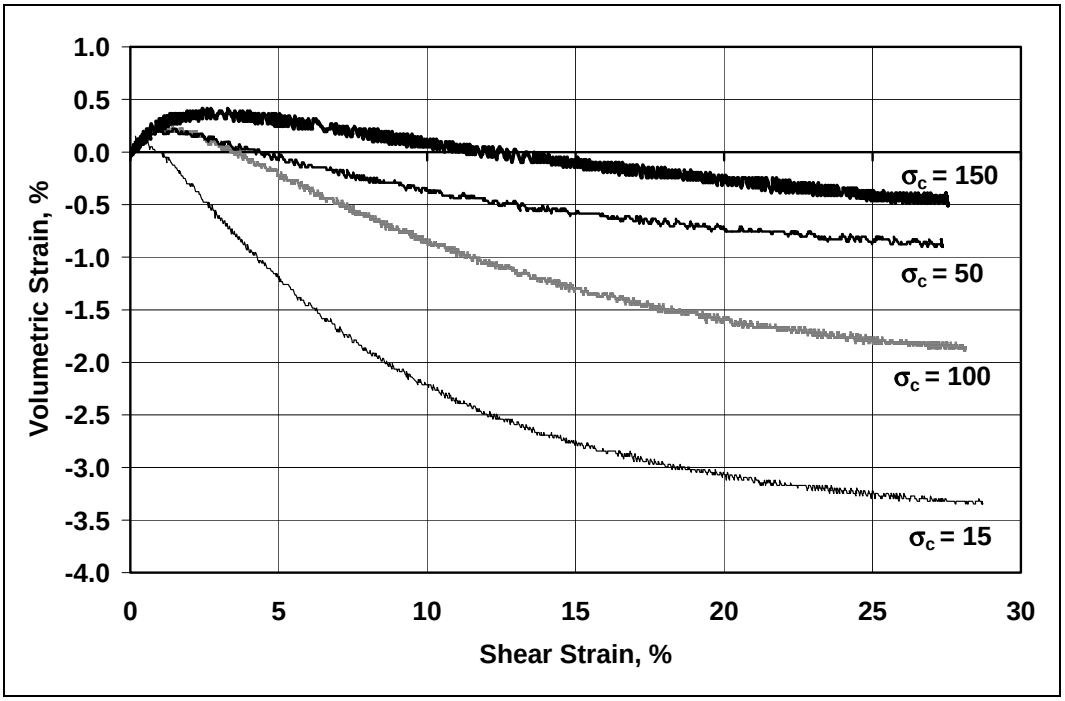

Figure 16. Drained volumetric strain–shear strain response for SP sand.

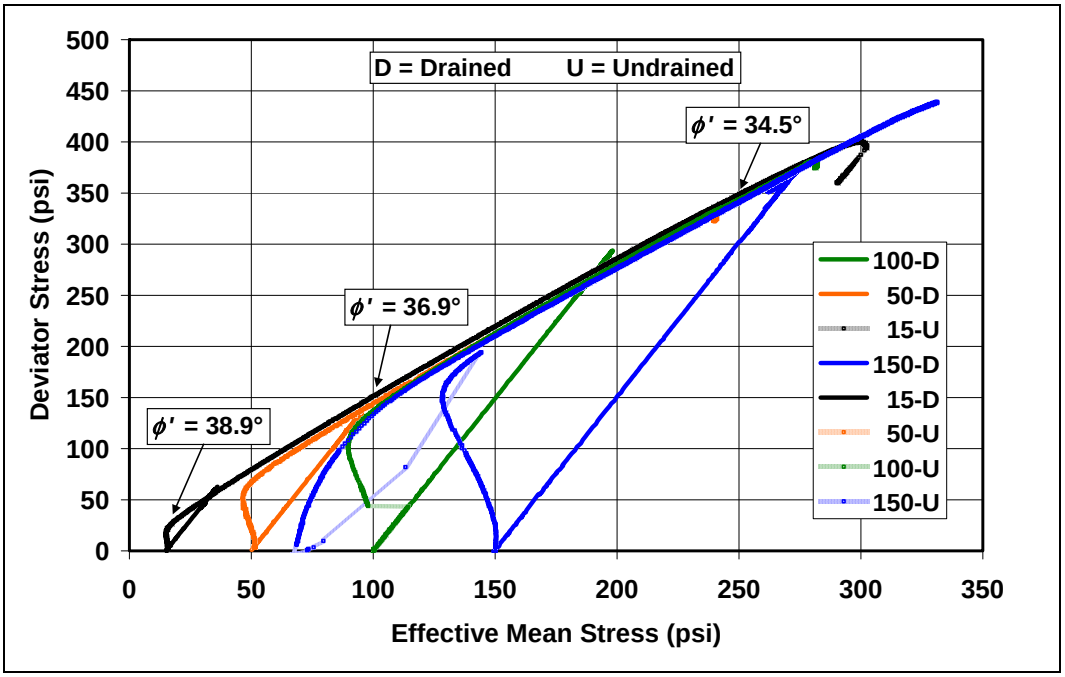

Figure 17. Effective stress paths for drained and undrained TX tests.

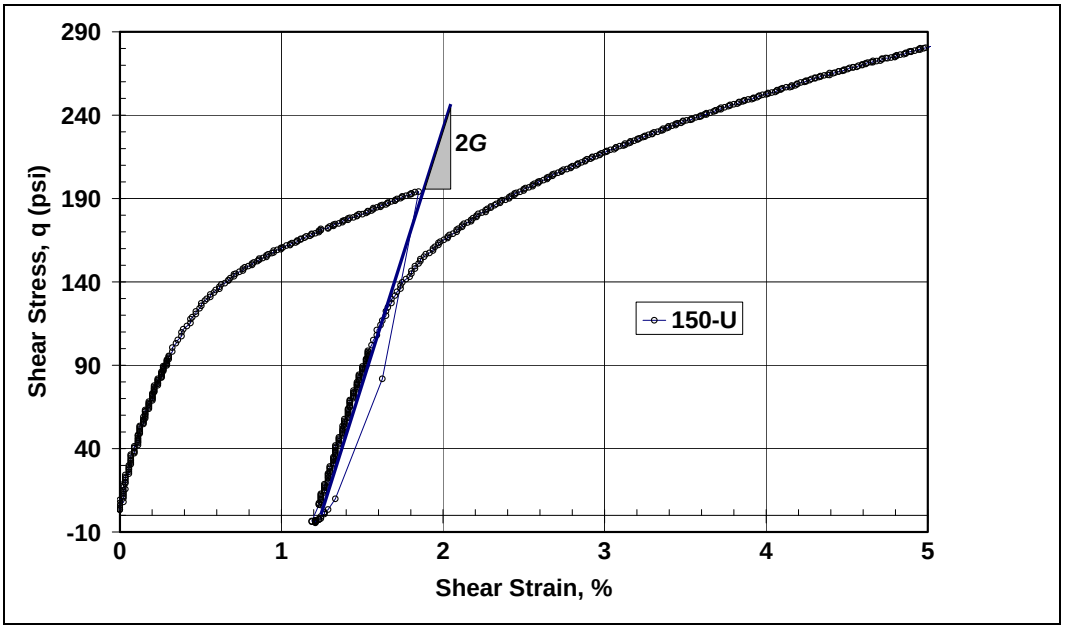

Figure 18. Hysteretic shear stress-strain response of SP sand at 150 psi confinement.

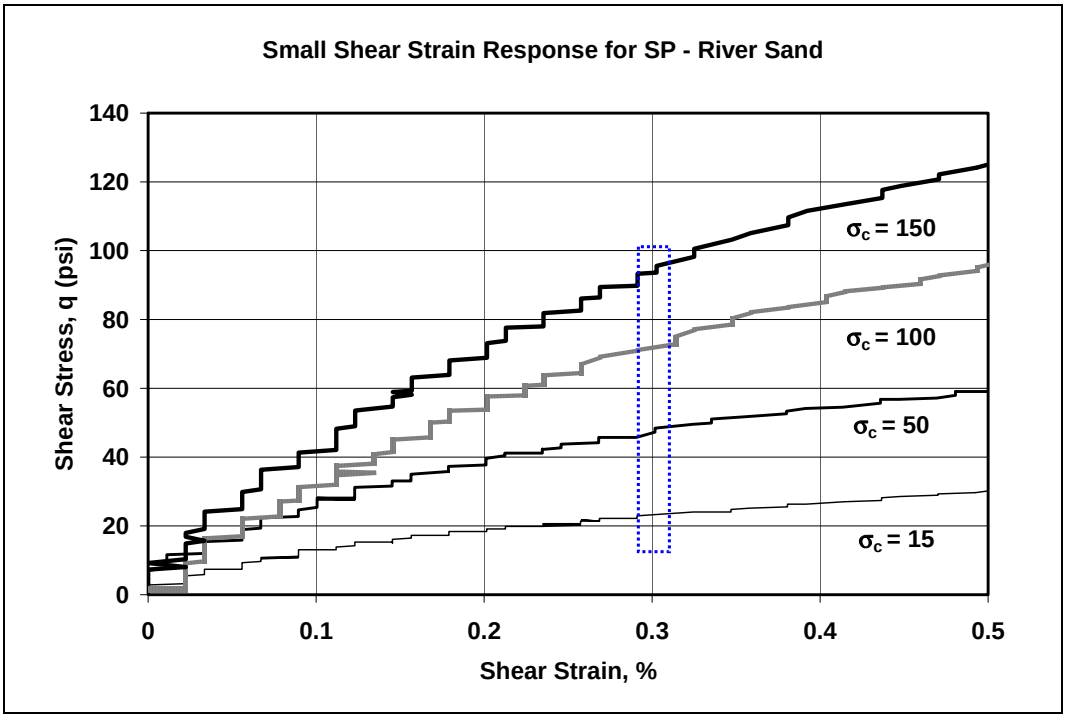

Figure 19. Small shear strain behavior of undrained triaxial tests

To provide a range of shear modulus as a function of effective mean stress, $\sigma'_m = (\sigma'_1 + 2\sigma'_3)/3$, G was calculated for each confining pressure at a strain level of 0.3% and plotted as a power law in Figure 20. This approach to estimating elastic moduli is common in the development of the hyperbolic model (Duncan and Chang 1970), with the exception that these relationships are based on effective mean stress versus solely the effective confining stress, σ'_3.

Granular soils exhibit an elastic Poisson's ratio, ν = 0.2 to 0.3 (Lambe and Whitman 1969). Using an average value of 0.25, the Young's modulus, E, for the concrete sand can be calculated as a function of confining pressure (as shown in Figure 20). For the case of the 150 psi confined sample, this would give a Young's modulus 0f 38,000 psi. A common relationship to estimate Young's modulus for soils (Heukelom and Foster 1960) is the expression E = 1500 * CBR (psi). From Figure 2, the sand at its compacted water content of 4% and standard Proctor density has a CBR of 25. This yields an estimated Young's modulus of 37,500 psi, agreeing well with the above data. This suggests that the E = 1500 * CBR function is valid for this concrete sand in future estimations of modulus behavior. It should be noted that, as CBR increases, the correlation with Young's modulus becomes less significant. For the ranges of CBR experienced by the concrete sand, a good semi-logarithmic fit between these two variables exists.

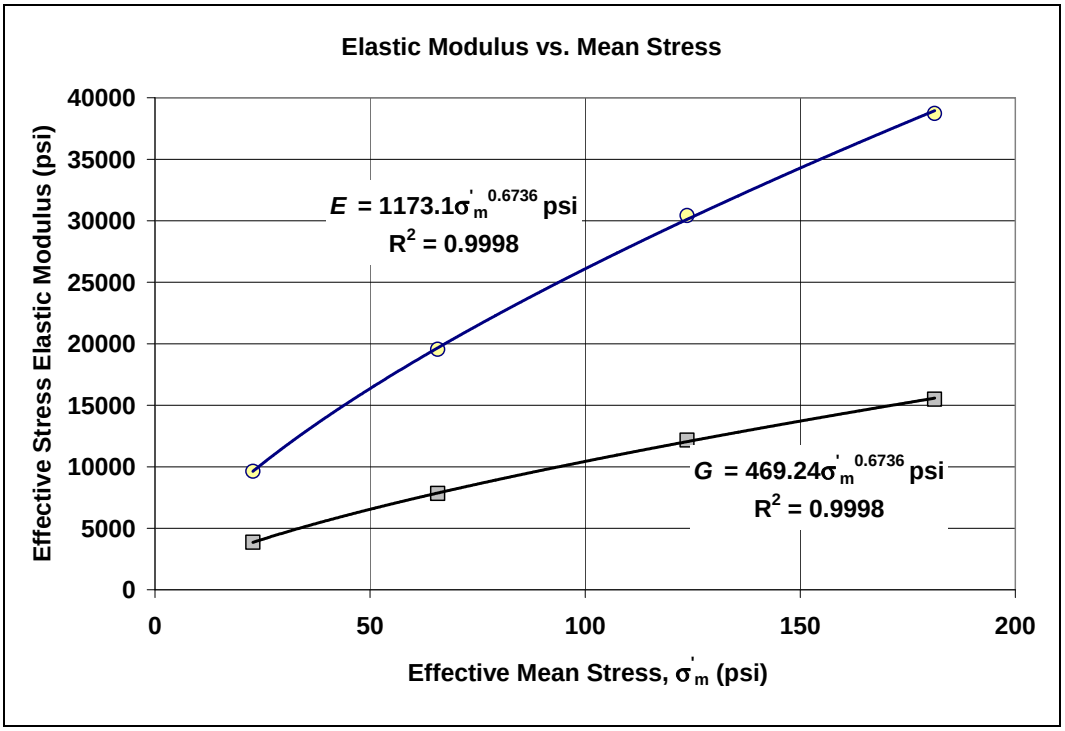

Figure 20. Elastic moduli as a function of effective mean stress

The effective stress path for concrete sand in Figure 17 illustrates that all the tests converge on a single yield surface. This yield surface is not linear as suggested by the direct shear data, but rather concave with an effective stress friction angle, ϕ', lying between 34 and 39 deg between the critical state condition and a highly dilative response, respectively. These values approximate the maximum and minimum friction angles determined from the direct shear tests, giving further confidence as to the anticipated range of friction angles. This plot also suggests that little to no cohesion exists for this SP material, which supports the fitting of the direct shear failure envelope through the origin of the stress plane to determine friction angle.

Partially saturated triaxial CU test (modified Q-test)

In order to provide data that would indicate the influence of the partial saturation on the constitutive response of the concrete sand (as is typical in a field in situ condition), a series of simple partially saturated triaxial tests were conducted at varying moisture contents. These tests were designed to simulate typical loading and drainage conditions in an in situ loading environment. Preparation of each specimen occurred in the same order as the saturated CU tests, with the exception that no water was drawn through the specimens. The specimens were left at their compacted moisture content prior to application of confining pressure. Initial

conditions of each prepared specimen are listed in Table 4 and labeled modified CU-Q tests.

Table 4. Initial conditions of modified CU-Q tests.

	Void Ratio			
Specimen	After Compaction	After Backsaturation	After Consolidation	After Shear
2%	0.551	0.551	0.551	0.551
3%	0.520	0.520	0.520	0.520
4%	0.536	0.536	0.536	0.536
5%	0.535	0.535	0.535	0.535
Average	0.536	0.536	0.536	0.536
Std. Dev.	0.013	0.013	0.013	0.013

At the beginning of each test, upper and lower drainage valves were opened to the atmosphere so that the air within the specimen could drain freely during the isotropic consolidation phase of the test. The chamber pressure was then increased to an effective confining pressure of 10 psi in a single increment. The confinement was necessary to prevent the sand specimen from collapsing prior to application of the axial load. The axial deformation of each specimen was measured, and no consolidation occurred during placement of the confining pressure.

At the end of consolidation phase, each specimen was sheared at a constant rate of axial displacement of 0.06 in./min. This loading rate will produce a 20% axial strain in 10 min. The drainage valves on each specimen were left open to allow free drainage of air within the specimen. The amount of water discharged from the specimens was not practical to measure as the rapid shearing of the CU test limited water flow out of the sample to zero.

A load cell was used to measure the vertical force applied to the specimen, and the chamber pressure was held constant providing a measurement of the total major and minor principal stresses. Figure 21 shows the resultant shear stress versus axial strain results for each of the four tests.

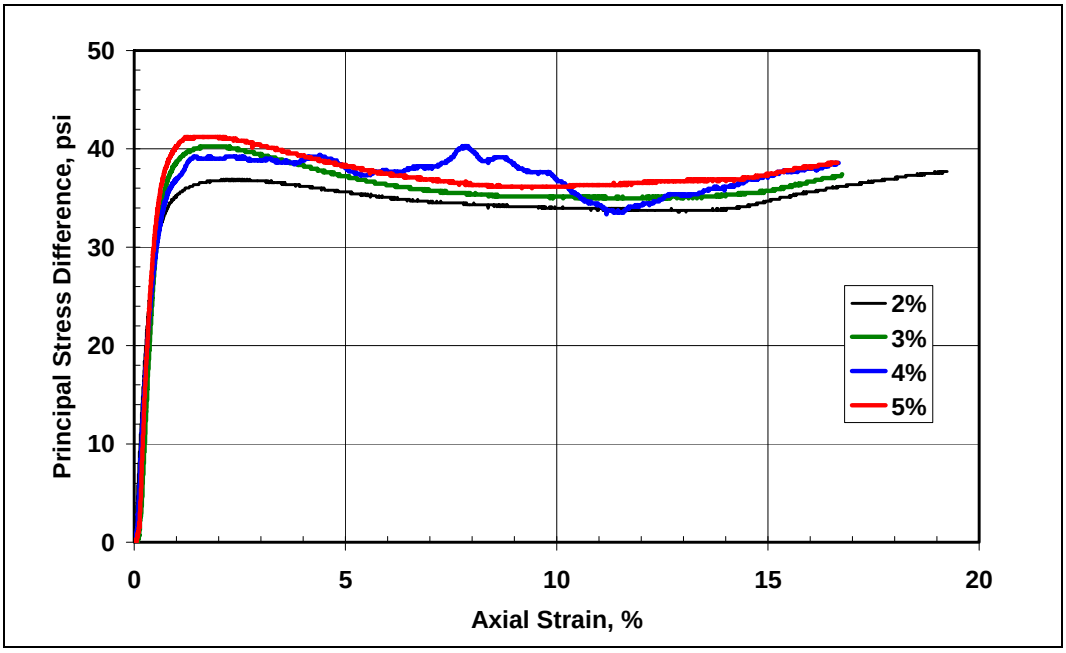

Figure 21. Modified CU-Q triaxial shear stress versus axial strain.

At the end of each test, chambers were relieved of pressure, and the entire specimen was dried and weighed to determine final water content. In the tests at 2, 3, and 4% water content, there was little to no change in final water content, suggesting that internal suction kept moisture migration from occurring in the samples. However, the post-test water content of the 5% specimen was only 3%, suggesting that some percentage of the water was mobile during shearing and, as such, was lost during the test.

Table 5 provides a summary of initial void ratio, water content, and peak deviator or shear strength response for each of the various tests. It should be noted that the initial density of each specimen is nearly the same. The results indicate that the shear strength of concrete sand is relatively insensitive to the effects of partial saturation since the principal stress at the same initial density does not vary with change in initial water content.

Table 5. Summary of modified CU-Q test strength results.

Modified CU-Q Test Data for SP Concrete Sand						
Nominal Water Content (%)	Void Ratio Before & After Consolidation	Final Water Content (%)	Dry Density (%)	Confining Pressure (psi)	Peak Shear Strength (psf)	q/2p
2	0.551	2.0	107.4	10	37.7	1.89
3	0.520	3.0	109.6	10	40.2	2.01
4	0.532	4.1	108.5	10	40.3	2.02
5	0.539	3.0	108.6	10	41.2	2.06

4 Summary and Conclusions

Summary of concrete sand properties

The data summarized below provide the means to determine a wide variety of material properties for use in modeling and validation of indirect physical testing of concrete sand. The following tabulations represent the mechanical properties determined from the laboratory investigations described in Chapters 1–3.

Classification:

USCS: SP – Poorly Graded Sand (nonplastic)
AASHTO: A-3
% Gravel: 6.3%
% Sand: 91.3%
% Fines: 2.4%
Specific Gravity: 2.66

Elastic properties:

Effective Stress Shear Modulus: $G = 469.24\ \sigma'_m{}^{0.6736}$ psi
Effective Stress Young's Modulus: $E = 1173.1\ \sigma'_m{}^{0.6736}$ psi
Poisson's Ratio: 0.25
Correlation between strength and Young's modulus:
$E = 1500 * \text{CBR}$

Effective stress strength properties:

Peak friction angle: 40°
Minimum friction angle: 32.8°
Average friction angle: 36.5°
Cohesion: 0 psi
Coefficient of consolidation, C_c: 0.03 (measured), 0.156 (Lee 1965)
Coefficient of reconsolidation, C_s: 0.01 (est. from isotropic data)
Undrained compressive strength at 10 psi confinement: 39.9 psi

Construction properties:

Maximum relative density: 114.1 pcf
Minimum relative density: 63.9 pcf
Maximum dry density (modified Proctor): 112.5 pcf
Optimum moisture content (modified Proctor): 2%
CBR at optimum conditions (dry): 38 (53 max)
Maximum dry density (standard Proctor): 111 pcf
Optimum moisture content (standard Proctor): 3% and 8%
CBR at optimum conditions (dry): 25 (at 3%), 16 (at 8%)

Recommendations

Determination of consolidation properties for granular materials is difficult because of the large pressures required to achieve steady-state deformation. Therefore, it is recommended that the coefficients of consolidation and reconsolidation be used with caution, with emphasis placed on the value determined by Lee that was obtained under pressures much greater than those used in this laboratory investigation.

References

Allen, W. A., E. B. Mayfield, and H. L. Morrison. 1957. Dynamics of a projectile penetrating sand. *Journal of Applied Physics* 28:370-376.

Anderson, W. W., T. J. Ahrens, A. Gibson, R. Scott, and K. Suzuki. 1996. Emplacement of penetrators into planetary surfaces. *Journal of Geophysical Research* 101(E9): 21137-21149.

Backman, M. E., and W. Goldsmith. 1978. The mechanics of penetration of projectiles into targets. *International Journal of Engineering Science* 16:1-99.

Black, W. P. M. 1961. The calculation of laboratory and in-situ values of California bearing ratio from bearing capacity data. *Geotechnique* 11:14-21.

Duncan, J. M., and A. L. Buchignani. 1976. *An engineering manual for settlement studies*. University of California, Berkeley: Department of Civil Engineering.

Duncan, J. M., and C. Chang. 1970. Nonlinear analysis of stress and strain in soils. *ASCE Journal of Soil Mechanics and Foundations* 96(SM5):1629-1653.

Gill, W. R. 1968. Influence of compaction hardening of soil on penetration resistance. In *Transactions for the American Society of Agricultural Engineers* 11:741-745.

Heukelom, W., and C. R. Foster. 1960. Dynamic testing of pavements. ASCE *Journal of the Soil Mechanics and Foundations Division* 86(SM1):1-28.

Johnson, J. B. 2001. A physically based penetration equation for compressible materials. In *Proceedings of the International Workshop on Penetrometry in the Solar System*, 18-20 October 1999, ed. N. I. Kömle, G. Kargl, A. J. Ball and R. D. Lorenz, 73-85. Graz, Austria: Österreichischen Akademie der Wissenschaften.

Lambe, W. T., and R. V. Whitman. 1969. *Soil mechanics*, New York: John Wiley and Sons.

Lee, K. L. 1965. *Triaxial compressive strength of saturated sand under seismic loading conditions.* University of California, Berkeley: Department of Civil Engineering.

Thompson, M. R., and Q. L. Robnett. 1979. Resilient properties of subgrade soils. *Journal of Transportation Engineering* 105:71-89. American Society of Civil Engineering.

Young, C. W. 1997. *Penetration equations.* Contractor Report SAND97-2426:24. Albuquerque, NM: Sandia National Laboratories.

REPORT DOCUMENTATION PAGE

Form Approved
OMB No. 0704-0188

1. REPORT DATE *(DD-MM-YYYY)*	2. REPORT TYPE	3. DATES COVERED *(From - To)*
February 2008	Final report	

4. TITLE AND SUBTITLE

Mechanical and Physical Properties of ASTM C33 Sand

5a. CONTRACT NUMBER

5b. GRANT NUMBER

5c. PROGRAM ELEMENT NUMBER

6. AUTHOR(S)

Ernest S. Berney IV and Donald M. Smith

5d. PROJECT NUMBER

5e. TASK NUMBER

5f. WORK UNIT NUMBER

7. PERFORMING ORGANIZATION NAME(S) AND ADDRESS(ES)

U.S. Army Engineer Research and Development Center
Geotechnical and Structures Laboratory
3909 Halls Ferry Road
Vicksburg, MS 39180-6199

8. PERFORMING ORGANIZATION REPORT NUMBER

ERDC/GSL TR-08-2

9. SPONSORING / MONITORING AGENCY NAME(S) AND ADDRESS(ES)

Headquarters, U.S. Army Corps of Engineers
Washington, DC 20314-1000

10. SPONSOR/MONITOR'S ACRONYM(S)

11. SPONSOR/MONITOR'S REPORT NUMBER(S)

12. DISTRIBUTION / AVAILABILITY STATEMENT

Approved for public release; distribution is unlimited.

13. SUPPLEMENTARY NOTES

14. ABSTRACT

Determining the state of the ground is critical for Objective Force operations. Currently, no methods exist to remotely, and accurately, measure the near-surface soil properties (strength, density, compressibility, and texture) needed to define ground state. Analysis of low-velocity impact probe deceleration, obtained during penetration, is the most practical method to remotely determine ground state. Development of the physics describing the behavior of the impact requires in-depth knowledge of the physical properties of the relevant soil. This report provides an extensive suite of calibration and verification material properties for predicting the response of an ASTM C33 sand to low-velocity probe penetration. The experimental program determined the following physical properties for this sand: elastic behavior (shear and Young's moduli and Poisson's ratio), strength characteristics (friction angle, cohesion, compressibility, and triaxial strength), and construction parameters (maximum/minimum densities, optimum moisture content, and California bearing ratio).

15. SUBJECT TERMS

Concrete aggregate
Elastic modulus
Partially saturated soil
Sand
Soil testing
Triaxial testing

16. SECURITY CLASSIFICATION OF:			17. LIMITATION OF ABSTRACT	18. NUMBER OF PAGES	19a. NAME OF RESPONSIBLE PERSON
a. REPORT	b. ABSTRACT	c. THIS PAGE			19b. TELEPHONE NUMBER *(include area code)*
UNCLASSIFIED	UNCLASSIFIED	UNCLASSIFIED		38	